Induction Motor Control With Friction Compensation: An Approach of Virtual-Desired-Variable Synthesis

Kuang-Yow Lian, *Member, IEEE*, Cheng-Yao Hung, Chian-Song Chiu, *Member, IEEE*, and Peter Liu

***Abstract*—In this paper, the speed control problem of induction motors suffering from substantial friction force is considered. Here, a *semi-current-fed* model for induction motors and LuGre's dynamic model for friction force are used. To reflect practical situations, rotor resistance, torque load, and friction parameters are assumed to be unknown. In the design methodology, a *double-observer* structure is applied to estimate the immeasurable friction states. On the other hand, in light of the principles of vector control and field orientation, a set of *virtual desired variables* (VDVs) are introduced to synthesize the control law. Therefore, using only measurable signals of rotor speed, stator voltage and current, an asymptotic adaptive tracking controller is designed. Numerical simulations and experiments are carried out to verify the theoretical results and show satisfactory performance.**

***Index Terms*—Adaptive control, friction force, induction motor, semi-current-fed model.**

I. Introduction

INDUCTION motors are highly reliable, rugged, easy to maintain and are of low cost. Therefore, its usage in speed and torque tracking control applications is expected to be quite popular in the near future [1]–[3]. A well-known and efficient method for the control of induction motors is called field orientation control [4], [5]. On the other hand, an induction motor driven by current control inverters which have high-gain current loops can assume the stator currents to be the control inputs. Under this assumption, an ideal current-fed model is derived [6]–[9]. From this ideal condition, the dynamic model of the induction motor can be reduced from a fifth order system to a third order one. Based on the reduced-model, the control design of induction motors is simplified. A typical research topic in current-fed induction motor control is the design of an output feedback approach [10], [11] to achieve speed and flux regulation. This is achieved in spite of both unknown time-varying rotor resistance and torque load. In this case, a rotor flux observer and a rotor resistance estimator form a complex bilinear estimation method. To cope with this, many control schemes have been proposed in [12]–[15].

Manuscript received July 17, 2003; revised October 14, 2004. This work was supported by the National Science Council, R.O.C, under Grant NSC-87-2213-E033-024. Recommended by Associate Editor B. Fahimi.

K.-Y. Lian and C.-Y. Hung are with the Department of Electrical Engineering, Chung-Yuan Christian University, Chung-Li 32023, Taiwan, R.O.C. (e-mail: lian@dec.ee.cycu.edu.tw).

C.-S. Chiu is with the Department of Electronic Engineering, Chien-Kuo Technology University, Changhua 50050, Taiwan, R.O.C. (e-mail: cschiu@cc.ctu.edu.tw).

P. Liu is with the BG Networking and Communications, BENQ Corporation, Taipei 114, Taiwan, R.O.C. (e-mail: petermliu@benq.com).

Digital Object Identifier 10.1109/TPEL.2005.854028

For mechanical systems, different degrees of friction force exist between two surfaces in contact. However in practical applications, friction is a very complicated phenomenon that relies on the physical properties of the contact surfaces, i.e., material properties and relative velocity. Therefore, a realistic friction model is employed to represent the dynamic friction existing in induction motors rather than only considering static viscous friction. All these static and dynamic characteristics of friction can be captured by the analytic LuGre model proposed in [16]. This dynamic model turns out to be suitable for the design of model-based friction compensation schemes without loss of generality. Numerous adaptive friction compensation schemes have been proposed [17]–[21].

In this paper, we propose a more practical *semi-current-fed* model for induction motors. Here, we either assume the current-loop maintains an upper bounded stator voltage and/or a bounded integral of current tracking error. This assumption is a relaxed version of the previous works on current-fed models where an ideal current-loop control is needed. To make practical considerations even more complete, the dynamic friction effect is described by a LuGre model. An adaptive scheme addressed in [17] is extended to handle nonuniform parametric variations of the friction force. According to the semi-current-fed model and the LuGre-based friction model, a nonlinear controller with adaptive friction compensation is proposed to achieve speed tracking. In the controller design, only the rotor speed, stator voltage and current are considered measurable while both rotor resistance and torque load are unknown. A set of virtual desired variables (VDVs) are defined and utilized to synthesize the adaptive controller. The VDVs are determined in a straightforward manner based on the goal of achieving both a well performed current regulator and exact field orientation. From Lyapunov stability analysis, the proposed adaptive controller is proven to achieve asymptotic speed tracking. In addition, if flux tracking is achieved the condition of persistent excitation (PE) is satisfied. From a robustness point of view, tracking errors with respect to current error has a finite gain L_2 stable relationship. This is the robust performance induced by the synthesis method. On the other hand, the adaptive mechanism imposed in the scheme can afford to keep low sensitivity to the change of parameter values. Hence, the variations such as rotor resistance fluctuations due to temperature are well coped with.

Based on the proposed control scheme, experiments are carried out to demonstrate the effect of friction compensation. A device with coarse surface is placed below the rotor shaft of the induction motor. This mechanism can produce substantial friction force. Then three scenarios are considered—**Case 1**: Rotor shaft without suffering friction force; **Case 2**: Rotor shaft suffering friction force *without* friction compensation; and **Case 3**: Rotor shaft suffering friction force *with* friction compensation.

From the comparison of experimental results, the effect of friction compensation for **Case 3** is nicely exhibited. This result is analogous to numerical simulations.

The rest of the paper is organized as follows. In Section II, we introduce the dynamic LuGre friction model, the semi-current-fed model, and the control objective. In Section III, the design method of VDV-synthesis is addressed. In Section IV, the adaptive controller and stability analysis are given. In Section V, the simulation and experimental results are given to verify the performance of the proposed controller. Finally, some conclusions are made in Section VI.

II. Problem Formulation

A. Dynamical Model of Induction Motors With Friction

Let $(i_{\rm sa}, i_{\rm sb}), (\lambda_{\rm ra}, \lambda_{\rm rb})$, and ω denote the components of the stator current, rotor flux, and rotor speed, respectively. The model of a three-phase induction motor is therefore represented by a fifth-order model [5]

$$\dot{i}_{\rm sa} = -\left(\frac{R_s}{\sigma} + \frac{L_m^2 R_r}{\sigma L_r^2}\right) i_{\rm sa} + \frac{L_m R_r}{\sigma L_r^2}\lambda_{\rm ra} + \frac{L_m}{\sigma L_r}\omega\lambda_{\rm rb} + \frac{1}{\sigma}V_{\rm sa} \tag{1}$$

$$\dot{i}_{\rm sb} = -\left(\frac{R_s}{\sigma} + \frac{L_m^2 R_r}{\sigma L_r^2}\right) i_{\rm sb} + \frac{L_m R_r}{\sigma L_r^2}\lambda_{\rm rb} - \frac{L_m}{\sigma L_r}\omega\lambda_{\rm ra} + \frac{1}{\sigma}V_{\rm sb} \tag{2}$$

$$\dot{\lambda}_{\rm ra} = \frac{L_m R_r}{L_r} i_{\rm sa} - \frac{R_r}{L_r}\lambda_{\rm ra} - \omega\lambda_{\rm rb} \tag{3}$$

$$\dot{\lambda}_{\rm rb} = \frac{L_m R_r}{L_r} i_{\rm sb} - \frac{R_r}{L_r}\lambda_{\rm rb} + \omega\lambda_{\rm ra} \tag{4}$$

$$J\dot{\omega} = T - T_l - F \tag{5}$$

where $(V_{\rm sa}, V_{\rm sb})$ denote the stator voltages; R_s, R_r, L_s, L_r, and L_m are the stator resistance, rotor resistance, stator inductance, rotor inductance, and mutual inductance, respectively; parameter $\sigma = L_s - L_m^2/L_r$; J, T_l, F are the mechanical inertia, loading torque, and friction force, respectively; and T is a scalar function representing the electromechanical coupling torque expressed as

$$T = \frac{n_p L_m}{L_r}(\lambda_{\rm ra} i_{\rm sb} - \lambda_{\rm rb} i_{\rm sa}) \tag{6}$$

where $n_p = (\text{pole pair}) \times (3/2)$. Furthermore, the varying friction force F is characterized by the LuGre friction model [16]

$$F = \sigma_0 z + \sigma_1 \frac{dz}{dt} + \sigma_2 \omega \tag{7}$$

$$\frac{dz}{dt} = \omega - \frac{|\omega|}{g(\omega)} z \tag{8}$$

where z is the friction state that physically reflects the average deflection of the bristles between two contact surfaces. The friction force parameters σ_0, σ_1, and σ_2 are the stiffness of bristles, damping coefficient, and viscous coefficient, respectively.

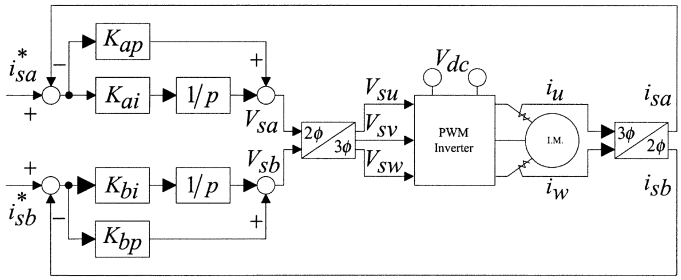

Fig. 1. Block diagram of current-fed induction motors.

Here, we assume that these three parameters are unknown positive constants. To describe the Stribeck effect, the parameterization of $g(\omega)$ is assumed with the following form:

$$g(\omega) = F_C + (F_S - F_C)e^{-\left(\frac{\omega}{\omega_s}\right)^2} \tag{9}$$

where F_C is the Coulomb friction value; F_S is the value of the stiction force; and ω_s is the Stribeck velocity. Notice that $g(\omega)$ is bounded and positive.

The dynamical model (1)–(6) expressed in a compact vector form is

$$\beta\dot{\mathbf{i}} + \left(\frac{L_r R_s}{L_m} + \frac{L_m R_r}{L_r}\right)\mathbf{i} + \left(\omega\mathbf{J}_2 - \frac{R_r}{L_r}\mathbf{I}_2\right)\boldsymbol{\lambda} = \frac{L_r}{L_m}\mathbf{V}_s \tag{10}$$

$$\dot{\boldsymbol{\lambda}} - \left(\omega\mathbf{J}_2 - \frac{R_r}{L_r}\mathbf{I}_2\right)\boldsymbol{\lambda} - \frac{L_m R_r}{L_r}\mathbf{i} = 0 \tag{11}$$

$$J\dot{\omega} = T - T_l - F \tag{12}$$

$$T = \frac{n_p L_m}{L_r}\mathbf{i}^{\rm T}\mathbf{J}_2\boldsymbol{\lambda} \tag{13}$$

where

$$\beta = \frac{\sigma L_r}{L_m}, \quad \mathbf{i} = \begin{bmatrix} i_{\rm sa} \\ i_{\rm sb} \end{bmatrix}, \quad \boldsymbol{\lambda} = \begin{bmatrix} \lambda_{\rm ra} \\ \lambda_{\rm rb} \end{bmatrix}, \quad \mathbf{V}_s = \begin{bmatrix} V_{\rm sa} \\ V_{\rm sb} \end{bmatrix},$$
$$\mathbf{I}_2 = \begin{bmatrix} 1 & 0 \\ 0 & 1 \end{bmatrix}, \quad \mathbf{J}_2 = \begin{bmatrix} 0 & -1 \\ 1 & 0 \end{bmatrix}.$$

B. Semi-Current-Fed Model

In practical current-fed induction motors, high-gain PI current loops regulate the stator currents. A concise block diagram of a current-fed induction motor system is shown in Fig. 1. The block diagram illustrates that the stator current $\mathbf{i}$ is forced to track the reference signal $\mathbf{i}^* = (i^*_{\rm sa}, i^*_{\rm sb})$ by virtue of the PI control inputs

$$V_{\rm sa} = -K_{\rm ap}(i_{\rm sa} - i^*_{\rm sa}) - K_{\rm ai}\int_0^t (i_{\rm sa} - i^*_{\rm sa})\,dt \tag{14}$$

$$V_{\rm sb} = -K_{\rm bp}(i_{\rm sb} - i^*_{\rm sb}) - K_{\rm bi}\int_0^t (i_{\rm sb} - i^*_{\rm sb})\,dt \tag{15}$$

where the positive gains $K_{\rm ap}, K_{\rm ai}, K_{\rm bp}$, and $K_{\rm bi}$ are properly chosen such that the current loop has perfect performance. Therefore, the dynamics of the stator currents (10) are neglected and the reference signals of the stator are regarded as the control inputs. In other words, $\mathbf{i}$ in (11) is replaced by

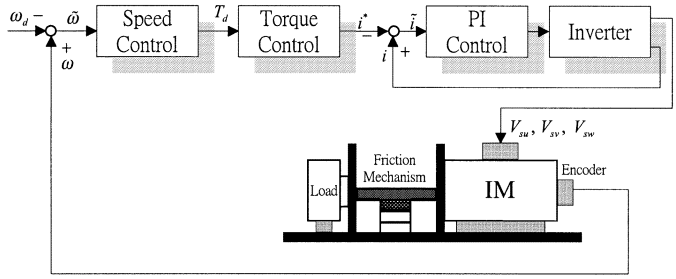

Fig. 2. Concept of control design for semi-current-fed induction motor.

the control input $\mathbf{i}^*$. Finally, the reduced-order model of the induction motor is expressed by (11) and (12).

However, due to current loop uncertainties and saturation phenomenon induced by high-gain control, the assumption of an ideal current loop in practical situations is not easily satisfied. To cope with this problem, a semi-current-fed concept is stated in the following assumptions.

A.1: By proper choice of PI gains in (14) and (15), the current loops perform well such that $\mathbf{V}_s$ is bounded, i.e., $\mathbf{V}_s \in L_\infty$.

Since (14) and (15) can be viewed as a stable filter driven by $\mathbf{V}_s$, we have $(\mathbf{i} - \mathbf{i}^*) \in L_\infty$ according to **A.1**. A stronger assumption is made as follows:

A.2: In addition to **A.1**, the current tracking errors are assumed to be finite integrable functions, i.e., $(\mathbf{i} - \mathbf{i}^*) \in L_\infty \cap L_1$.

In light of **A.1** or **A.2**, we call this a semi-current-fed induction motor. This terminology arises from the fact that **A.1** and **A.2** relax the typical ideal current-fed induction motor control assumptions $i_{\rm sa} = i^*_{\rm sa}, i_{\rm sb} = i^*_{\rm sb}$. Therefore the speed control design based on a semi-current-fed concept is closer to practical situations.

Before the controller synthesis, the problem is formulated in light of the following scenarios.

S.1 The voltages and currents of stator, along with the velocity of rotor are measurable.

S.2 Moment of inertia J and load torque T_l are unknown constants.

S.3 The parameters, L_m, L_r, R_s, are known constants whereas R_r is unknown.

S.4 The desired speed ω_d is a smooth and bounded function.

III. Controller Synthesis by Virtual Desired Variables

A. Mechanical Loop Control

The concept of control design for a semi-current-fed induction motor is shown in Fig. 2. First, let us consider the mechanical dynamics (12), which is rewritten in terms of the speed tracking error

$$J\dot{\tilde{\omega}} + B\tilde{\omega} = T - T_l - J\dot{\omega}_d - B\omega_d - \sigma_0 z + \sigma_1 \frac{|\omega|}{g(\omega)} z \quad (16)$$

where $B \equiv \sigma_1 + \sigma_2 > 0$ and $\tilde{\omega} \equiv \omega - \omega_d$. Note that the friction state z is not measurable and parameters σ_0, σ_1 are unknown. Therefore, we will attempt to reconstruct the friction state through the use of two observers [17]. Denote the states of the two observers as $\hat{z}_0$ and $\hat{z}_1$. We construct the observers as

$$\frac{d\hat{z}_0}{dt} = \omega - \frac{|\omega|}{g(\omega)}\hat{z}_0 + \iota_0 \quad (17)$$

$$\frac{d\hat{z}_1}{dt} = \omega - \frac{|\omega|}{g(\omega)}\hat{z}_1 + \iota_1 \quad (18)$$

where ι_0, ι_1 are compensation terms to be determined later. From (8), the corresponding estimation errors

$$\frac{d\tilde{z}_0}{dt} = -\frac{|\omega|}{g(\omega)}\tilde{z}_0 - \iota_0 \quad (19)$$

$$\frac{d\tilde{z}_1}{dt} = -\frac{|\omega|}{g(\omega)}\tilde{z}_1 - \iota_1 \quad (20)$$

where $\tilde{z}_0 = z - \hat{z}_0$ and $\tilde{z}_1 = z - \hat{z}_1$. In light of this, (16) is further written as

$$J\dot{\tilde{\omega}} + (B + k_\omega)\tilde{\omega} = T - T_d + \Big[T_d - \mathbf{Y}\boldsymbol{\theta} + k_\omega\tilde{\omega} - \sigma_0(\tilde{z}_0 + \hat{z}_0) + \sigma_1\frac{|\omega|}{g(\omega)}(\tilde{z}_1 + \hat{z}_1)\Big] \quad (21)$$

where T_d denotes the desired torque which produces the desired speed; k_ω is an adjustable damping ratio; $\mathbf{Y} = [1 \;\; \dot{\omega}_d \;\; \omega_d]$ is a regression matrix; and $\boldsymbol{\theta} \equiv [T_l \;\; J \;\; B]^T$ is a parameter vector. The damping term $k_\omega\tilde{\omega}$ plays a dominant role on the transient response for speed tracking. From (21), we choose

$$T_d = \mathbf{Y}\hat{\boldsymbol{\theta}} - k_\omega\tilde{\omega} + \hat{\sigma}_0\hat{z}_0 - \frac{|\omega|}{g(\omega)}\hat{\sigma}_1\hat{z}_1 \quad (22)$$

where $\hat{\boldsymbol{\theta}}$ is the estimated vector of $\boldsymbol{\theta}$; $\hat{\sigma}_0$, and $\hat{\sigma}_1$ are the estimated values of σ_0, and σ_1, respectively. Therefore the following error dynamics is obtained:

$$J\dot{\tilde{\omega}} + (B + k_\omega)\tilde{\omega} = T - T_d - \mathbf{Y}\tilde{\boldsymbol{\theta}} - \sigma_0\tilde{z}_0 - \tilde{\sigma}_0\hat{z}_0 + \sigma_1\frac{|\omega|}{g(\omega)}\tilde{z}_1 + \tilde{\sigma}_1\frac{|\omega|}{g(\omega)}\hat{z}_1 \quad (23)$$

with the estimation error $\tilde{\boldsymbol{\theta}} \equiv \boldsymbol{\theta} - \hat{\boldsymbol{\theta}}$. The update laws for $\hat{\boldsymbol{\theta}}, \hat{\sigma}_0$, and $\hat{\sigma}_1$ will be properly chosen such that the terms containing $\tilde{\boldsymbol{\theta}}, \tilde{z}_0$, and $\tilde{z}_1$ are driven to zero. Therefore the rotor speed will converge to the desired value at a desired rate based on a suitably chosen k_ω if T approaches T_d. At this point, the speed tracking control problem has been reformulated into the torque tracking problem. In other words, the remainder of the control design is to generate a torque T to track the desired torque T_d while all internal signals are maintained bounded.

B. VDV-Synthesis

Although the following method is somewhat similar to the well-known backstepping control [22], the highly coupled nonlinearity of induction motors makes the typical backstepping methodology not straightforward. To cope with this problem, the concept of virtual desired variables (VDVs) is introduced.

The VDV-synthesis is carried out for the semi-current fed model

$$\dot{\boldsymbol{\lambda}} - \left(\omega\mathbf{J}_2 - \frac{R_r}{L_r}\mathbf{I}_2\right)\boldsymbol{\lambda} = \frac{L_m R_r}{L_r}\mathbf{i}^*. \quad (24)$$

According to the principle of vector control, our goal is to design $\mathbf{i}^*$ and a virtual desired flux $\boldsymbol{\lambda}_d$ independently such that the electrical subsystem can generate the desired torque T_d. According to the torque (13), we synthesize

$$T_d = \frac{n_p L_m}{L_r} \mathbf{i}^{*\mathrm{T}} \mathbf{J}_2 \boldsymbol{\lambda}_d. \tag{25}$$

Therefore, once $\mathbf{i}$ and $\boldsymbol{\lambda}$ converge correspondingly to $\mathbf{i}^*$ and $\boldsymbol{\lambda}_d, T$ converges to T_d. Based on the semi-current-fed concept, the convergence of $\mathbf{i}$ to $\mathbf{i}^*$ depends on whether the current loop controller satisfies the assumptions $\mathbf{A.1}$ or $\mathbf{A.2}$. Consequently, the objective of torque tracking is reformulated into designing $\mathbf{i}^*$ and $\boldsymbol{\lambda}_d$ such that $\boldsymbol{\lambda} \to \boldsymbol{\lambda}_d$ while satisfying (25). In light of vector control analysis, we note that the optimal torque is obtained if the magnitude of rotor flux is kept constant. As a result, we will attempt to design $\mathbf{i}^*$ such that $\boldsymbol{\lambda} \to \boldsymbol{\lambda}_d$, whereas $\boldsymbol{\lambda}_d$ and $\mathbf{i}^*$ are subject to the following conditions.

- $\mathbf{C.1}$ Flux $\boldsymbol{\lambda}_d$ is kept constant by letting $\|\boldsymbol{\lambda}_d\| = c$, where c is a given constant.
- $\mathbf{C.2}$ Flux $\boldsymbol{\lambda}_d$ and current $\mathbf{i}^*$ satisfy (25).

The condition $\mathbf{C.1}$ implies that the virtual desired flux in the stator frame is $\boldsymbol{\lambda}_d = (c\cos(\rho(t)) \; c\sin(\rho(t)))$, where $\rho(t)$ denotes the angle, to be determined later, with respect to the stator frame.

C. Realization of VDV-Synthesis

Since the rotor flux is immeasurable, the direct constructive approach is not trivial. Compared to observer-based methodology, an alternative approach is used here. We investigate (10) and (11), and obtain

$$\beta \dot{\mathbf{i}} + \dot{\boldsymbol{\lambda}} = \dot{\boldsymbol{\eta}} \tag{26}$$

where $\boldsymbol{\eta}$ is a first-order filter defined as

$$\dot{\boldsymbol{\eta}} = -\frac{L_r R_s}{L_m} \mathbf{i} + \frac{L_r}{L_m} \mathbf{V}_s.$$

Integrating (26), the flux signals satisfy

$$\boldsymbol{\lambda} = \boldsymbol{\eta} - \beta \mathbf{i} + \mathbf{A} \tag{27}$$

where $\mathbf{A}$ is an unknown integration constant vector dependent on initial conditions. From (27), the reconstructed flux signals are expressed as $\hat{\boldsymbol{\lambda}} = \boldsymbol{\eta} - \beta \mathbf{i} + \hat{\mathbf{A}}$, where $\hat{\mathbf{A}}$ is an estimated signal of $\mathbf{A}$ and is to be determined by the adaptive mechanism. The remaining VDV-synthesis algorithm is given in the following.

Step1 Replace the original flux tracking problem with the tracking of reconstructed flux. Define the tracking error of reconstructed flux, error of estimated rotor resistance, and error of estimated integration constant, accordingly as $\tilde{\boldsymbol{\lambda}} = \hat{\boldsymbol{\lambda}} - \boldsymbol{\lambda}_d$, $\tilde{R}_r = R_r - \hat{R}_r$, and $\tilde{\mathbf{A}} = \mathbf{A} - \hat{\mathbf{A}}$, where $\hat{R}_r$ is the estimated rotor resistance. From (11), we obtain

$$\begin{aligned}
\dot{\tilde{\boldsymbol{\lambda}}} &= \dot{\boldsymbol{\lambda}} + \dot{\hat{\mathbf{A}}} - \dot{\boldsymbol{\lambda}}_d \\
&= \left(\omega \mathbf{J}_2 - \frac{R_r}{L_r} \mathbf{I}_2\right)(\hat{\boldsymbol{\lambda}} + \tilde{\mathbf{A}}) + \frac{L_m}{L_r} R_r \mathbf{i} + \dot{\hat{\mathbf{A}}} - \dot{\boldsymbol{\lambda}}_d \\
&= \left(\omega \mathbf{J}_2 - \frac{R_r}{L_r} \mathbf{I}_2 - \frac{L_m R_r}{L_r} k_\lambda\right) \tilde{\boldsymbol{\lambda}} + \tilde{R}_r \boldsymbol{\phi}_r + \omega \mathbf{J}_2 \tilde{\mathbf{A}} \\
&\quad - \tilde{\mathbf{B}} + \frac{L_m}{L_r} R_r \tilde{\mathbf{i}} + \boldsymbol{\xi}_\lambda - \boldsymbol{\varsigma}
\end{aligned} \tag{28}$$

where $\tilde{\mathbf{i}} \equiv \mathbf{i} - \mathbf{i}^*; \tilde{\mathbf{B}} \equiv \mathbf{B} - \hat{\mathbf{B}}$ ($\hat{\mathbf{B}}$ is the estimated signal of $\mathbf{B} \equiv \frac{R_r}{L_r}\mathbf{A}$); $k_\lambda > 0; \boldsymbol{\varsigma}$ is an auxiliary signal determined later; and

$$\begin{aligned}
\boldsymbol{\xi}_\lambda &= \left(\omega \mathbf{J}_2 - \frac{\hat{R}_r}{L_r} \mathbf{I}_2\right) \boldsymbol{\lambda}_d + \frac{L_m \hat{R}_r}{L_r} k_\lambda \tilde{\boldsymbol{\lambda}} - \hat{\mathbf{B}} \\
&\quad + \frac{\hat{R}_r}{L_r} \hat{\mathbf{A}} + \frac{L_m}{L_r} \hat{R}_r \mathbf{i}^* + \dot{\hat{\mathbf{A}}} - \dot{\boldsymbol{\lambda}}_d + \boldsymbol{\varsigma} \\
\boldsymbol{\phi}_r &= \frac{L_m}{L_r} \mathbf{i}^* - \frac{1}{L_r} \boldsymbol{\lambda}_d + \frac{1}{L_r} \hat{\mathbf{A}} + \frac{L_m}{L_r} k_\lambda \tilde{\boldsymbol{\lambda}}.
\end{aligned}$$

Since all the signals in $\boldsymbol{\xi}_\lambda$ are available, we set $\boldsymbol{\xi}_\lambda = 0$ to determine $\mathbf{i}^*$. From definition of $\boldsymbol{\lambda}_d$, we obtain

$$\begin{aligned}
\mathbf{i}^* = \frac{L_r}{L_m \hat{R}_r}&((\dot{\rho} - \omega) \mathbf{J}_2 \boldsymbol{\lambda}_d + \hat{\mathbf{B}} - \dot{\hat{\mathbf{A}}} - \boldsymbol{\varsigma}) \\
&- \frac{1}{L_m}(\hat{\mathbf{A}} - \boldsymbol{\lambda}_d) - k_\lambda \tilde{\boldsymbol{\lambda}}
\end{aligned} \tag{29}$$

where the relation $\dot{\boldsymbol{\lambda}}_d = \dot{\rho}(t) \mathbf{J}_2 \boldsymbol{\lambda}_d$ (cf., C.1) has been used.

Step2 Substitute (29) into (25) (i.e., satisfying C.2). Then along with C.1, the angle $\rho(t)$ is determined

$$\begin{aligned}
\dot{\rho}(t) = \omega + \frac{1}{c^2}\Bigg(\hat{R}_r\Bigg(\frac{T_d}{n_p} + \frac{L_m}{L_r} k_\lambda \tilde{\boldsymbol{\lambda}}^{\mathrm{T}} \mathbf{J}_2 \boldsymbol{\lambda}_d + \frac{1}{L_r} \hat{\mathbf{A}}^{\mathrm{T}} \mathbf{J}_2 \boldsymbol{\lambda}_d\Bigg) \\
+ (\dot{\hat{\mathbf{A}}} + \boldsymbol{\varsigma} - \hat{\mathbf{B}})^{\mathrm{T}} \mathbf{J}_2 \boldsymbol{\lambda}_d\Bigg).
\end{aligned} \tag{30}$$

Therefore, $\mathbf{i}^*$ can be rewritten in terms of T_d

$$\begin{aligned}
\mathbf{i}^* = \frac{1}{L_m}&\left(\mathbf{I}_2 + \frac{1}{c^2} \psi \mathbf{J}_2\right) \boldsymbol{\lambda}_d \\
&+ \frac{L_r}{L_m \times \hat{R}_r}(\hat{\mathbf{B}} - \dot{\hat{\mathbf{A}}} - \boldsymbol{\varsigma}) - k_\lambda \tilde{\boldsymbol{\lambda}} - \frac{1}{L_m} \hat{\mathbf{A}}
\end{aligned} \tag{31}$$

where

$$\begin{aligned}
\psi = (L_m k_\lambda \tilde{\boldsymbol{\lambda}} + \hat{\mathbf{A}})^{\mathrm{T}} \mathbf{J}_2 \boldsymbol{\lambda}_d \\
+ L_r \left(\frac{T_d}{n_p} + \frac{1}{\hat{R}_r}(\dot{\hat{\mathbf{A}}} + \boldsymbol{\varsigma} - \hat{\mathbf{B}})^{\mathrm{T}} \mathbf{J}_2 \boldsymbol{\lambda}_d\right).
\end{aligned}$$

Hence, $\boldsymbol{\lambda}_d$ and $\mathbf{i}^*$ have been defined.

IV. Adaptive Mechanism and Stability Analysis

In this section, we define the update laws for all parameter estimations and carry out the stability analysis for the overall system. Based on the control law (31), the error dynamics (23) and (28) are further expressed as

$$\begin{aligned}
J\dot{\tilde{\omega}} + (B + k_\omega)\tilde{\omega} = \frac{L_m n_p}{L_r}(\mathbf{i}^{\mathrm{T}} \mathbf{J}_2 \tilde{\boldsymbol{\lambda}} + \mathbf{i}^{\mathrm{T}} \mathbf{J}_2 \tilde{\mathbf{A}} + \tilde{\mathbf{i}}^{\mathrm{T}} \mathbf{J}_2 \boldsymbol{\lambda}_d) - \mathbf{Y}\tilde{\boldsymbol{\theta}} \\
- \sigma_0 \tilde{z}_0 - \tilde{\sigma}_0 \hat{z}_0 + \sigma_1 \frac{|\omega|}{g(\omega)} \tilde{z}_1 + \tilde{\sigma}_1 \frac{|\omega|}{g(\omega)} \hat{z}_1
\end{aligned} \tag{32}$$

$$\begin{aligned}
\dot{\tilde{\boldsymbol{\lambda}}} = \left(\omega \mathbf{J}_2 - \frac{R_r}{L_r} \mathbf{I}_2 - \frac{L_m R_r}{L_r} k_\lambda \mathbf{I}_2\right) \tilde{\boldsymbol{\lambda}} + \tilde{R}_r \boldsymbol{\phi}_r \\
+ \omega \mathbf{J}_2 \tilde{\mathbf{A}} - \tilde{\mathbf{B}} + \frac{L_m}{L_r} R_r \tilde{\mathbf{i}} - \boldsymbol{\varsigma}
\end{aligned} \tag{33}$$

where (13) and (25) have been used. In the following, we show that the tracking errors $\tilde{\omega}$ and $\tilde{\boldsymbol{\lambda}}$ are convergent once update

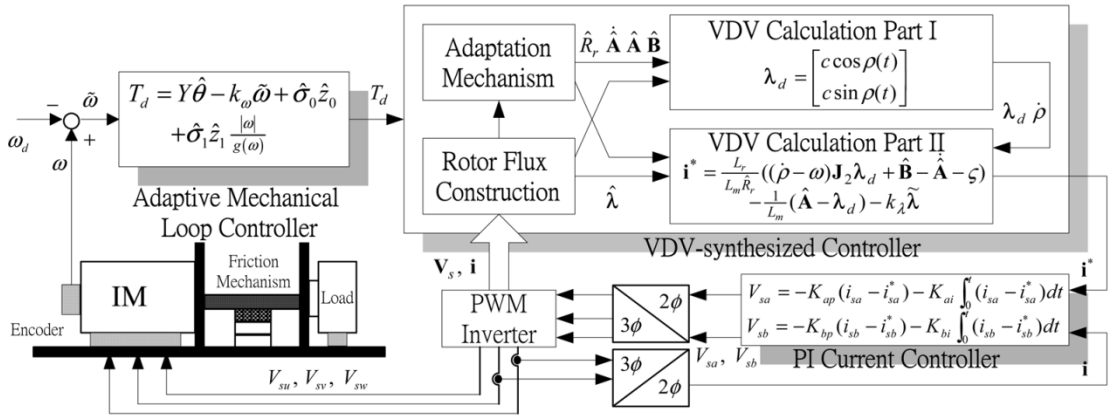

Fig. 3. Structure of the adaptive controller.

laws for $\hat{R}_r, \hat{\boldsymbol{\theta}}, \hat{\mathbf{A}}, \hat{\mathbf{B}}, \hat{\sigma}_0$, and $\hat{\sigma}_1$ are suitably chosen. Consider a Lyapunov function candidate as

$$V = \frac{1}{2}\alpha J\tilde{\omega}^2 + \frac{1}{2}\alpha\tilde{\boldsymbol{\theta}}^{\mathrm{T}}\boldsymbol{\Gamma}_4^{-1}\tilde{\boldsymbol{\theta}} + \frac{1}{2}\left(\tilde{\boldsymbol{\lambda}}^{\mathrm{T}}\tilde{\boldsymbol{\lambda}} + \gamma_1^{-1}\tilde{R}_r^2 + \tilde{\mathbf{A}}^{\mathrm{T}}\boldsymbol{\Gamma}_2^{-1}\tilde{\mathbf{A}} + \tilde{\mathbf{B}}^{\mathrm{T}}\boldsymbol{\Gamma}_3^{-1}\tilde{\mathbf{B}} + \gamma_5^{-1}\tilde{\sigma}_0^2 + \gamma_6^{-1}\tilde{\sigma}_1^2\right) + \frac{1}{2}\sigma_0\tilde{z}_0^2 + \frac{1}{2}\sigma_1\tilde{z}_1^2 \tag{34}$$

where α is an arbitrary positive constant; and $\gamma_1, \boldsymbol{\Gamma}_2 = \boldsymbol{\Gamma}_2^{\mathrm{T}}, \boldsymbol{\Gamma}_3 = \boldsymbol{\Gamma}_3^{\mathrm{T}}, \boldsymbol{\Gamma}_4 = \boldsymbol{\Gamma}_4^{\mathrm{T}}, \gamma_5, \gamma_6$, are positive definite adaptation gains. Using (32) and (33), the derivative of (34) with respect to time leads to

$$\begin{aligned}\dot{V} = &-\alpha(B+k_\omega)\tilde{\omega}^2 - \frac{R_r}{L_r}(1+L_m k_\lambda)\tilde{\boldsymbol{\lambda}}^{\mathrm{T}}\tilde{\boldsymbol{\lambda}} \\ &+ \tilde{R}_r(\gamma_1^{-1}\dot{\tilde{R}}_r + \tilde{\boldsymbol{\lambda}}^{\mathrm{T}}\boldsymbol{\phi}_r) \\ &+ \tilde{\mathbf{A}}^{\mathrm{T}}\left(\boldsymbol{\Gamma}_2^{-1}\dot{\tilde{\mathbf{A}}} + \frac{\alpha L_m n_p}{L_r}\tilde{\omega}\mathbf{J}_2^{\mathrm{T}}\mathbf{i} + \omega\mathbf{J}_2^{\mathrm{T}}\tilde{\boldsymbol{\lambda}}\right) + \tilde{\mathbf{B}}^{\mathrm{T}}\left(\boldsymbol{\Gamma}_3^{-1}\dot{\tilde{\mathbf{B}}} - \tilde{\boldsymbol{\lambda}}\right) \\ &+ \alpha\tilde{\boldsymbol{\theta}}^{\mathrm{T}}\left(\boldsymbol{\Gamma}_4^{-1}\dot{\tilde{\boldsymbol{\theta}}} - \tilde{\omega}\mathbf{Y}^{\mathrm{T}}\right) + \tilde{\boldsymbol{\lambda}}^{\mathrm{T}}\left(\frac{\alpha L_m n_p}{L_r}\tilde{\omega}\mathbf{J}_2^{\mathrm{T}}\mathbf{i} - \boldsymbol{\varsigma}\right) \\ &+ \frac{L_m}{L_r}\tilde{\mathbf{i}}^{\mathrm{T}}(\alpha n_p\tilde{\omega}\mathbf{J}_2\boldsymbol{\lambda}_d + R_r\tilde{\boldsymbol{\lambda}}) \\ &+ \tilde{\sigma}_0\left(\gamma_5^{-1}\dot{\tilde{\sigma}}_0 - \alpha\tilde{\omega}\hat{z}_0\right) + \tilde{\sigma}_1\left(\gamma_6^{-1}\dot{\tilde{\sigma}}_1 + \alpha\tilde{\omega}\frac{|\omega|}{g(\omega)}\hat{z}_1\right) \\ &- \sigma_0\tilde{z}_0(\alpha\tilde{\omega} + \iota_0) \\ &+ \sigma_1\tilde{z}_1\left(\frac{|\omega|}{g(\omega)}\alpha\tilde{\omega} - \iota_1\right) - \sigma_0\frac{|\omega|}{g(\omega)}\tilde{z}_0^2 - \sigma_1\frac{|\omega|}{g(\omega)}\tilde{z}_1^2.\end{aligned}$$

To achieve a negative $\dot{V}$, the update law of $\hat{R}_r$ is chosen as

$$\dot{\hat{R}}_r = \begin{cases} 0, & \text{if } \hat{R}_r = R_0 \text{ and } \tilde{\boldsymbol{\lambda}}^{\mathrm{T}}\phi_r < 0 \\ \gamma_1\tilde{\boldsymbol{\lambda}}^{\mathrm{T}}\boldsymbol{\phi}_r, & \text{otherwise} \end{cases} \tag{35}$$

where R_0 denotes a lower bound of the unknown rotor resistance R_r. The update law for the estimation $\hat{R}_r$ satisfies

$$\tilde{R}_r\left(\gamma_1^{-1}\dot{\tilde{R}}_r + \tilde{\boldsymbol{\lambda}}^{\mathrm{T}}\boldsymbol{\phi}_r\right) = -\tilde{R}_r\gamma_1^{-1}(\dot{\hat{R}}_r - \gamma_1\tilde{\boldsymbol{\lambda}}^{\mathrm{T}}\boldsymbol{\phi}_r) \le 0$$

since $R_r > R_0$. The projection-type update law adopted here is to keep $\hat{R}_r$, which is present in the denominator of (29), bounded away from zero. The other update laws for $\hat{\mathbf{A}}, \hat{\mathbf{B}}, \hat{\boldsymbol{\theta}}, \hat{\boldsymbol{\sigma}}_0$, and $\hat{\boldsymbol{\sigma}}_1$ are

$$\dot{\hat{\mathbf{A}}} = \boldsymbol{\Gamma}_2\left(\frac{\alpha L_m n_p}{L_r}\tilde{\omega}\mathbf{J}_2^{\mathrm{T}}\mathbf{i} + \omega\mathbf{J}_2^{\mathrm{T}}\tilde{\boldsymbol{\lambda}}\right) \tag{36}$$

$$\dot{\hat{\mathbf{B}}} = -\boldsymbol{\Gamma}_3\tilde{\boldsymbol{\lambda}} \tag{37}$$

$$\dot{\hat{\boldsymbol{\theta}}} = -\tilde{\omega}\boldsymbol{\Gamma}_4\mathbf{Y}^{\mathrm{T}} \tag{38}$$

$$\dot{\hat{\sigma}}_0 = -\gamma_5\alpha\tilde{\omega}\hat{z}_0 \tag{39}$$

$$\dot{\hat{\sigma}}_1 = \gamma_6\alpha\tilde{\omega}\frac{|\omega|}{g(\omega)}\hat{z}_1. \tag{40}$$

Accordingly, the observer compensation terms are defined by

$$\iota_0 = -\alpha\tilde{\omega} \tag{41}$$

$$\iota_1 = \frac{|\omega|}{g(\omega)}\alpha\tilde{\omega} \tag{42}$$

where the auxiliary signal $\boldsymbol{\varsigma}$ is given as

$$\boldsymbol{\varsigma} = \frac{\alpha L_m n_p}{L_r}\tilde{\omega}\mathbf{J}_2^{\mathrm{T}}\mathbf{i}. \tag{43}$$

As a result, we arrive with the following equation:

$$\begin{aligned}\dot{V} = &-\alpha(B+k_\omega)\tilde{\omega}^2 - \frac{R_r}{L_r}(1+L_m k_\lambda)\tilde{\boldsymbol{\lambda}}^{\mathrm{T}}\tilde{\boldsymbol{\lambda}} \\ &+ \frac{L_m}{L_r}\tilde{\mathbf{i}}^{\mathrm{T}}[\alpha n_p\mathbf{J}_2\boldsymbol{\lambda}_d \quad R_r\mathbf{I}_2]\begin{bmatrix}\tilde{\omega} \\ \tilde{\boldsymbol{\lambda}}\end{bmatrix} - \sigma_0\frac{|\omega|}{g(\omega)}\tilde{z}_0^2 \\ &- \sigma_1\frac{|\omega|}{g(\omega)}\tilde{z}_1^2.\end{aligned} \tag{44}$$

The overall structure of the control law and the update laws for control parameters is illustrated in Fig. 3. The main results for the adaptive speed controller are summarized in the following.

Theorem 1: Consider a semi-current-fed induction motor with friction force variation characterized by (7)–(8). Here, we use the control law (31); dual observers (17), (18), (41), (42); desired torque (22); auxiliary signal (43); and the parameter update laws (35)–(40). If the control gains k_ω, k_λ, c, and α are suitably chosen, the closed-loop control system has the following properties.

a) If A.1 is satisfied, all signals in the closed-loop system are bounded. Furthermore, the tracking errors $\tilde{\omega}$ and $\tilde{\boldsymbol{\lambda}}$ with respect to the current error $\tilde{\mathbf{i}}$ is finite-gain L_2 stable, i.e.,

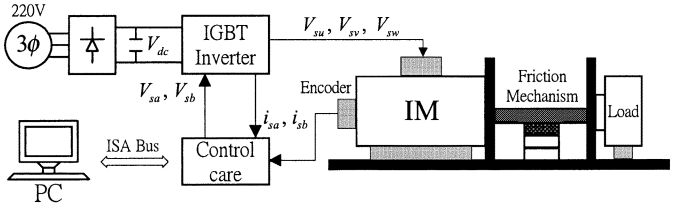

Fig. 4. Experimental setup.

$\int_0^t \|\mathbf{h}(\tau)\|^2 d\tau \le \epsilon_1 + \epsilon_2 \int_0^t \|\tilde{\mathbf{i}}(\tau)\|^2 d\tau$ for $\mathbf{h} = [\tilde{\omega}\ \tilde{\boldsymbol{\lambda}}^{\mathrm{T}}]^{\mathrm{T}}$ and some positive constants ϵ_1, ϵ_2.

b) If A.2 is satisfied, then the tracking errors $\tilde{\omega}$ and $\tilde{\boldsymbol{\lambda}}$ asymptotically converge to zero as $t \to \infty$.

Proof: See the Appendix. ■

Here we notice that the result of the theorem still holds even though the persistent excitation (PE) condition for internal signals is not satisfied. However, in this case, $\boldsymbol{\lambda}$ does not coverage to $\boldsymbol{\lambda}_d$ as $t \to \infty$. Nevertheless, asymptotical speed tracking is achieved.

Since the rotor flux tracking error $(\boldsymbol{\lambda} - \boldsymbol{\lambda}_d)$ equals to $(\tilde{\boldsymbol{\lambda}} + \tilde{\mathbf{A}})$, we need $\tilde{\mathbf{A}} \to 0$ to achieve $\boldsymbol{\lambda} \to \boldsymbol{\lambda}_d$ as $t \to \infty$. In traditional adaptive approaches [22], [23], zero parameter errors are obtained only if the PE condition is satisfied, thus the equation shown at the bottom of this page. If $\mathbf{W}(t)$ satisfies the PE condition, i.e., there exist two positive constants ν and μ such that

$$\int_t^{t+\nu} \mathbf{W}(\tau)\mathbf{W}^{\mathrm{T}}(\tau)d\tau \ge \mu\mathbf{I} > 0, \quad \forall t \ge 0$$

then asymptotic flux tracking will be achieved, that is, $\lim_{t\to\infty}(\boldsymbol{\lambda} - \boldsymbol{\lambda}_d) = 0$.

The optimal torque is generated if $\|\boldsymbol{\lambda}\|$ is kept constant. Therefore, the optimal torque property will be sustained if PE condition is satisfied.

V. Simulation and Experimental Results

In this section, the performance of the control scheme will be verified by numerical simulations and experiments. For comparison, numerical simulation results are put next to associated experiments results. The experimental setup is shown in Fig. 4. Here we emphasize that a mechanism with rough surface is added below the rotor shaft to produce a frictional force. The specifications and parameters of the induction motor are listed in Table I. For the friction model, parameters $F_c = 0.285, F_s = 0.335$, and $\omega_s = 0.01$ [3], [17], [21]. The induction motor is driven by a PC-based DSP controller. The software uses MATLAB Simulink Toolbox with Real Time Workshop Toolbox. Thoroughly considering all possible combinations, we breakdown scenarios based on speed command type and friction effect. In Table II, we list the friction effect scenarios. The overall execution time interval is set as 10 s for both simulations and experiments.

TABLE I
Specification and Parameters of the Induction Motor

Rated Specification	
Pole Pair	3
Power	0.4 kW
Voltage	120 V
Current	3.4 A
Speed	1500 rpm
Parameters	
R_s	2.85 Ω
R_r	4.0 Ω
L_s	0.19667 H
L_r	0.19667 H
L_m	0.1886 H
J	0.001 $kg-m^2$

TABLE II
Three Cases of the Proposed Scheme

	Friction Force	Friction Compensation
Case 1	Not Applied	Not Applied
Case 2	Applied	Not Applied
Case 3	Applied	Applied

Step-Type Command: Consider a smooth step-type speed command as $[30, 0, -30, 0]$ rad/s (dotted lines in Fig. 5) varied accordingly at time [0, 3, 5, 8] s. The control parameters are chosen as: $k_p = 500, k_i = 350, \alpha = 0.045, k_\omega = 1.5, k_\lambda = 0.2$, and $c = 0.41$. Update gains are set as $\boldsymbol{\Gamma}_1 = 5.5, \boldsymbol{\Gamma}_2 = \mathrm{diag}\{0.8, 0.8\}, \boldsymbol{\Gamma}_3 = \mathrm{diag}\{0.2, 0.2\}, \boldsymbol{\Gamma}_4 = \mathrm{diag}\{0.1, 6e^{-7}, 0.0046\}$. When friction compensation is activated, the update gains are set as: $\boldsymbol{\Gamma}_4 = \mathrm{diag}\{0.1, 6e^{-7}, 0.02\}, \boldsymbol{\Gamma}_5 = 10, \boldsymbol{\Gamma}_6 = 0.82$.

The simulation and experiment results of step-type command for **Case 1, Case 2, Case 3**, and tracking error of **Case 3** are shown in Fig. 5(a)–(d), respectively. For **Case 3**, the stator voltage, current for one phase and the estimated rotor resistance $\hat{R}_r$ are shown in Fig. 6(a)–(c), respectively.

Speed Tracking: Consider tracking of speed $\omega_d = 30 + 10\sin 2\pi t$ rad/s. The control parameters are chosen as: $k_p = 700, k_i = 350, \alpha = 0.05, k_\omega = 1.5, k_\lambda = 0.2$, and $c = 0.41$. Update gains are set as $\boldsymbol{\Gamma}_1 = 5.5, \boldsymbol{\Gamma}_2 = \mathrm{diag}\{0.8, 0.8\}, \boldsymbol{\Gamma}_3 = \mathrm{diag}\{0.2, 0.2\}, \boldsymbol{\Gamma}_4 = \mathrm{diag}\{0.1, 6e^{-7}, 0.000\,92\}$. When friction compensation is activated, the update gains are set as: $\boldsymbol{\Gamma}_4 = \mathrm{diag}\{0.1, 6e^{-7}, 0.02\}, \boldsymbol{\Gamma}_5 = 2, \boldsymbol{\Gamma}_6 = 0.82$.

The simulation and experiment results of speed tracking for **Case 1, Case 2, Case 3**, and tracking error of **Case 3** are shown in Fig. 7(a)–(d), respectively. For **Case 3**, the stator voltage,

$$\mathbf{W}^{\mathrm{T}}(t) = \begin{bmatrix} 0 & \frac{\alpha L_m n_p}{L_r}\mathbf{i}^{\mathrm{T}}\mathbf{J}_2 & 0 & -\alpha\mathbf{Y} & -\alpha\hat{z}_0 & \frac{|\omega|}{g(\omega)}\alpha\hat{z}_1 \\ \boldsymbol{\phi}_r & \omega\mathbf{J}_2 & -\mathbf{I}_2 & 0 & 0 & 0 \end{bmatrix}.$$

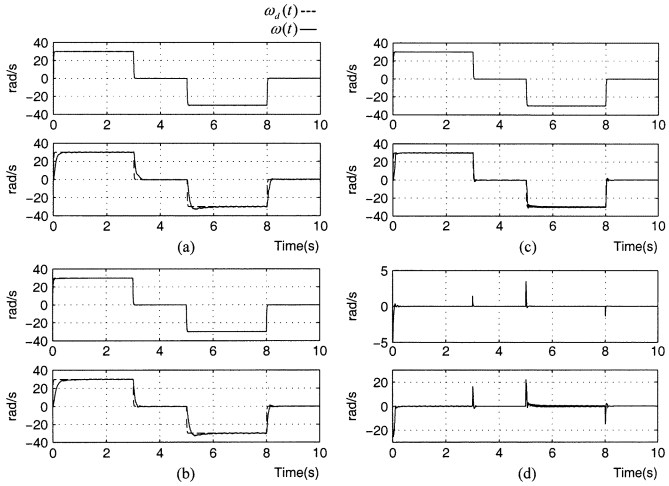

Fig. 5. Simulation and experimental results of step-type command for: (a) Case 1, (b) Case 2, (c) Case 3, and (d) tracking error of Case 3.

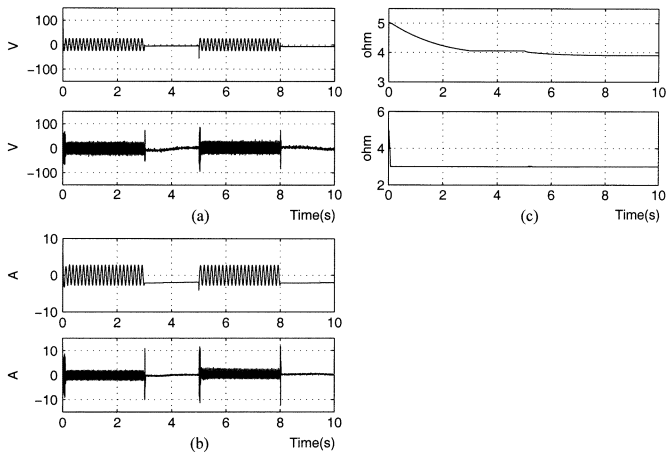

Fig. 6. Simulation and experimental results for Case 3: (a) stator voltage for one phase, (b) stator current for one phase, and (c) estimated rotor resistance.

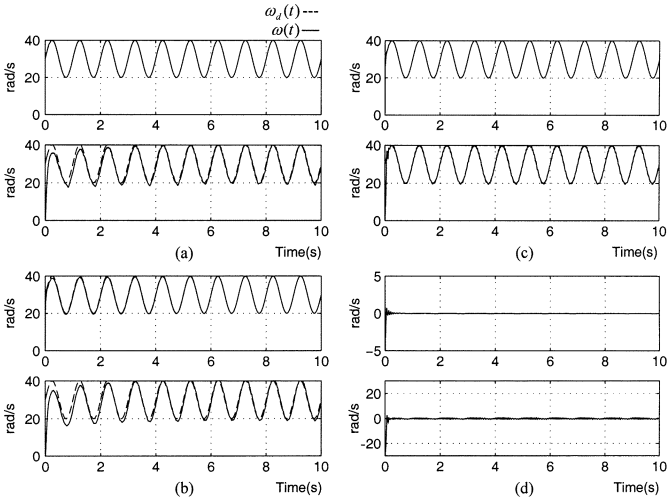

Fig. 7. Simulation and experimental results of speed tracking for: (a) Case 1, (b) Case 2, (c) Case 3, and (d) tracking error of Case 3.

current for one phase and the estimated rotor resistance $\hat{R}_r$ are shown in Fig. 8(a)–(c), respectively.

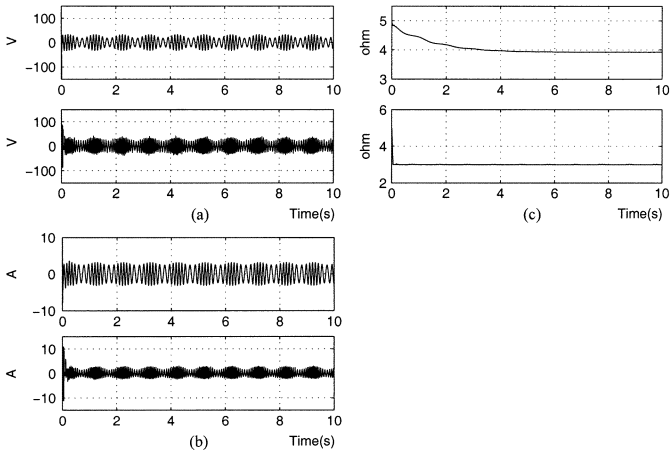

Fig. 8. Simulation and experimental results for Case 3: (a) stator voltage for one phase, (b) stator current for one phase, and (c) estimated rotor resistance.

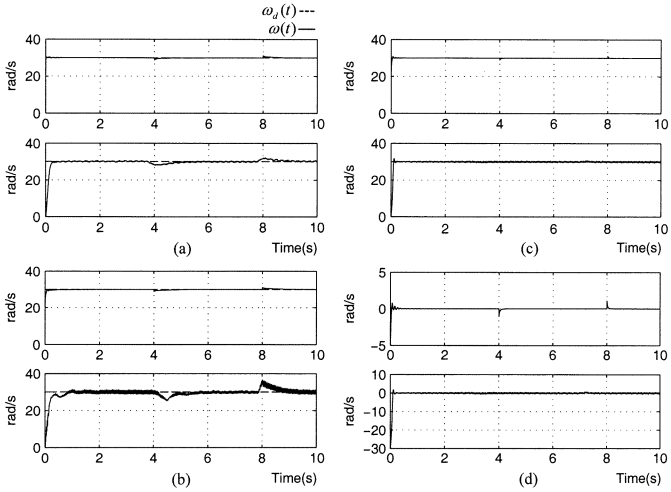

Fig. 9. Simulation and experimental results of regulation command with abrupt load variation for: (a) Case 1, (b) Case 2, (c) Case 3, and (d) tracking error of Case 3.

Regulation Command With Abrupt Load Variation: Consider speed regulation with abrupt load variation. An extra load 1.8 N·m is added at $t = 4$ s and removed at $t = 8$ s. The control parameters are chosen as: $k_p = 450, k_i = 350, \alpha = 0.055, k_\omega = 1.5, k_\lambda = 0.2$, and $c = 0.41$. Update gains are set as $\mathbf{\Gamma}_1 = 5.5, \mathbf{\Gamma}_2 = \mathrm{diag}\{0.8, 0.8\}, \mathbf{\Gamma}_3 = \mathrm{diag}\{0.2, 0.2\}, \mathbf{\Gamma}_4 = \mathrm{diag}\{0.1, 6e^{-7}, 0.0046\}$. When friction compensation is activated, the update gains are set as: $\mathbf{\Gamma}_4 = \mathrm{diag}\{0.1, 6e^{-7}, 0.02\}, \mathbf{\Gamma}_5 = 10, \mathbf{\Gamma}_6 = 0.82$.

The simulation and experiment results of regulation with abrupt load variation for **Case 1, Case 2, Case 3**, and tracking error of **Case 3** are shown in Fig. 9(a)–(d), respectively. For **Case 3**, the stator voltage, current for one phase and the estimated rotor resistance $\hat{R}_r$ are shown in Fig. 10(a)–(c), respectively.

Remark 1: To emphasize that our approach is robust from a practical point of view, we illustrate a PI controller (a Semi-Drive system default PI)-based IM system with speed regulation objectives for **Case 1** and **Case 2** friction scenarios. When load is abruptly changed, we can see that performance in Fig. 11 is worse than that of Fig. 9.

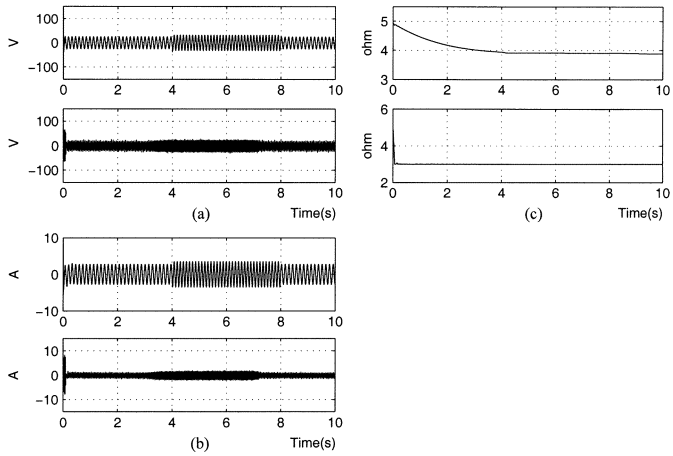

Fig. 10. Simulation and experimental results for Case 3: (a) stator voltage for one phase, (b) stator current for one phase, and (c) estimated rotor resistance.

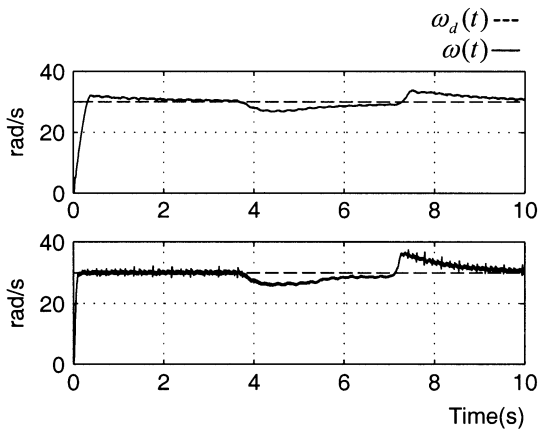

Fig. 11. Experimental results for Case 1 and Case 2 using PI controller.

VI. Conclusion

In this paper, we consider the speed tracking control with friction compensation for an induction motor. The induction motor is modeled by a *semi-current-fed* model whereas the frictional force is represented by a LuGre's dynamic model. Then an adaptive controller is designed by VDV-synthesis. From the numerical simulations and experimental results, we can see that when considering friction compensation, the performance is greatly improved. The satisfactory overshoot, transient behavior, and steady-state error are even better than the case when no friction force is applied. The proposed scheme can be further applied to the full fifth-order model of induction motors although the controller will become more complicated.

Appendix

Before proving **Theorem 1**, the following **Lemma 1** is introduced.

Lemma 1: The friction state is bounded if the rotor speed is bounded.

Proof: Considering the friction dynamics (8), we choose $V_z = \frac{1}{2}z^2$. Then

$$\dot{V}_z = z\omega - \frac{|\omega|}{g(\omega)}z^2 \leq -|z\omega|\left(\frac{|z|}{g(\omega)} - 1\right).$$

Since $\dot{V}_z$ is negative for $|z| > g(\omega)$, it is concluded that z is bounded. ■

Proof of **Theorem 1**:

Part (a): Since σ_0, σ_1 are positive constants and the friction characteristic function $g(\omega)$ is chosen to be a positive function, (44) leads to the following inequality:

$$\dot{V} \leq -\varepsilon\|\mathbf{h}\|^2 + k\|\tilde{\mathbf{i}}\|\|\mathbf{h}\| \tag{45}$$

where $\varepsilon = \min(\alpha(B + k_\omega), (R_r/L_r)(1 + L_m k_\lambda))$, and $k = (L_m/L_r)\sup_t \|[\alpha n_p \mathbf{J}_2\boldsymbol{\lambda}_d \;\; R_r\mathbf{I}_2]\| < \infty$. Here the norm of matrix $(L_m/L_r)[\alpha n_p\mathbf{J}_2\boldsymbol{\lambda}_d \;\; R_r\mathbf{I}_2]$ depends on c, (which is the magnitude of virtual desired flux) and electrical parameters L_r, L_m, R_r. Therefore k is bounded above by a constant. Consequently, if $\|\mathbf{h}\| \geq (k\|\tilde{\mathbf{i}}\|/\delta\varepsilon)$, then

$$\begin{aligned}\dot{V} &\leq -(1-\delta)\varepsilon\|\mathbf{h}\|^2 - \delta\varepsilon\|\mathbf{h}\|^2 + k\|\tilde{\mathbf{i}}\|\|\mathbf{h}\| \\ &\leq -(1-\delta)\varepsilon\|\mathbf{h}\|^2 \end{aligned} \tag{46}$$

where $0 < \delta < 1$. Since $\tilde{\mathbf{i}} \in L_\infty$, we conclude that V is upper bounded. Hence the error signals $\tilde{\omega}, \tilde{\boldsymbol{\lambda}} \in L_\infty$; observer errors $\tilde{z}_0, \tilde{z}_1 \in L_\infty$; and all parametric errors $\tilde{R}_r, \tilde{\mathbf{A}}, \tilde{\mathbf{B}}, \tilde{\boldsymbol{\theta}}, \tilde{\sigma}_0, \tilde{\sigma}_1 \in L_\infty$. Since $\boldsymbol{\lambda}_d, R_r, \mathbf{A}, \mathbf{B}, \boldsymbol{\theta}, \sigma_0, \sigma_1$ are constant, the parameter estimates $\hat{\boldsymbol{\lambda}}, \hat{R}_r, \hat{\mathbf{A}}, \hat{\mathbf{B}}, \hat{\boldsymbol{\theta}}, \hat{\sigma}_0, \hat{\sigma}_1 \in L_\infty$. Similarly, ω is bounded since naturally ω_d is a bounded desired speed. According to **Lemma 1**, the bounded $\tilde{z}_0, \tilde{z}_1$ induce that the observer states $\hat{z}_0, \hat{z}_1$ are bounded. Due to $\boldsymbol{\lambda} = \hat{\boldsymbol{\lambda}} + \tilde{\boldsymbol{\lambda}}$ and $\hat{\boldsymbol{\lambda}}, \tilde{\boldsymbol{\lambda}} \in L_\infty$, the rotor flux $\boldsymbol{\lambda}$ is therefore bounded. Therefore, the following remains to investigate the boundedness of signals $\mathbf{i}^*$ and $\dot{\rho}(t)$. Consider the dynamics of the stator current (10) rewritten as

$$\beta\dot{\mathbf{i}} + \left(\frac{L_r R_s}{L_m} + \frac{L_m R_r}{L_r}\right)\mathbf{i} = -\left(\omega\mathbf{J}_2 - \frac{R_r}{L_r}\mathbf{I}_2\right)\boldsymbol{\lambda} + \frac{L_r}{L_m}\mathbf{V}_s. \tag{47}$$

From assumption **A.1** and the fact $\omega, \boldsymbol{\lambda}, \mathbf{V}_s \in L_\infty$, the right-hand side of (47) is bounded. The dynamics (47) can be taken as a stable filter driven by the terms on the right-hand side. Hence, $\mathbf{i} \in L_\infty$. Considering (44) and the facts

$$\frac{\alpha L_m n_p}{L_r}\tilde{\omega}\tilde{\mathbf{i}}^{\mathrm{T}}\mathbf{J}_2\boldsymbol{\lambda}_d \leq \frac{\alpha^2 c^2 n_p^2}{R_r}\tilde{\omega}^2 + \frac{L_m^2 R_r}{4L_r^2}\tilde{\mathbf{i}}^{\mathrm{T}}\tilde{\mathbf{i}}$$

$$\frac{L_m R_r}{L_r}\tilde{\mathbf{i}}^{\mathrm{T}}\tilde{\boldsymbol{\lambda}} \leq R_r\tilde{\boldsymbol{\lambda}}^{\mathrm{T}}\tilde{\boldsymbol{\lambda}} + \frac{L_m^2 R_r}{4L_r^2}\tilde{\mathbf{i}}^{\mathrm{T}}\tilde{\mathbf{i}}$$

we are able to rewrite $\dot{V}$ as

$$\begin{aligned}\dot{V} &\leq -\alpha\left(B + k_\omega - \frac{\alpha c^2 n_p^2}{R_r}\right)\tilde{\omega}^2 \\ &\quad - \frac{R_r}{L_r}(1 + L_m k_\lambda - L_r)\tilde{\boldsymbol{\lambda}}^{\mathrm{T}}\tilde{\boldsymbol{\lambda}} + \frac{L_m^2 R_r}{2L_r^2}\|\tilde{\mathbf{i}}\|^2 \\ &= -\mathbf{h}^{\mathrm{T}}\mathbf{Q}\mathbf{h} + \frac{L_m^2 R_r}{2L_r^2}\|\tilde{\mathbf{i}}\|^2 \end{aligned} \tag{48}$$

where

$$\mathbf{Q} = \mathrm{diag}\left\{\alpha\left(B + k_\omega - \frac{\alpha c^2 n_p^2}{R_r}\right), \frac{R_r}{L_r}(1 + L_m k_\lambda - L_r)\mathbf{I}_2\right\}.$$

Note that $\mathbf{Q}$ is positive definite by choosing k_ω, k_λ, c, and α properly. Integrating on both sides of (48) leads to

$$\int_0^t \mathbf{h}^{\mathrm{T}}\mathbf{Q}\mathbf{h}d\tau \le V(0) - V(t) + \frac{L_m^2 R_r}{2L_r^2}\int_0^t \|\tilde{\mathbf{i}}\|^2 d\tau \le V(0) + \frac{L_m^2 R_r}{2L_r^2}\int_0^t \|\tilde{\mathbf{i}}\|^2 d\tau \quad (49)$$

and thus completes the proof of (a). ■

Part (b): From assumption **A.2**, we have $\tilde{\mathbf{i}} \in L_2$. In light of the result of Part (a), we have $\mathbf{h} \in L_2$ by (49). In addition, the fact $\dot{\mathbf{h}} \in L_\infty$ is concluded since all signals on the right-hand sides of (32) and (33) are bounded. According to $\mathbf{h}, \dot{\mathbf{h}} \in L_\infty, \mathbf{h} \in L_2$ and applying Barbalat's lemma [23], we have $\lim_{t\to\infty} \mathbf{h}(t)$. In other words, $\tilde{\omega}$ and $\tilde{\boldsymbol{\lambda}}$ asymptotically converges to zero as $t \to \infty$. ■

REFERENCES

[1] J. H. Yang, W. H. Yu, and L. C. Fu, "Nonlinear observer-based adaptive tracking control for induction motors with unknown load," *IEEE Trans. Ind. Electron.*, vol. 42, no. 6, pp. 579–586, Dec. 1995.

[2] A. M. Lee, L. C. Fu, C. Y. Tsai, and Y. C. Lin, "Nonlinear adaptive speed and torque control of induction motors with unknown rotor resistance," *IEEE Trans. Ind. Electron.*, vol. 48, no. 2, pp. 391–401, Apr. 2001.

[3] K. Y. Lian, C. Y. Hung, J. J. Liou, and P. Liu, "Adaptive speed control with friction compensation for semi-current-fed induction motors," in *Proc. 15th IFAC World Congr.*, Barcelona, Spain, 2002.

[4] A. M. Trzynadlowski, *The Field Orientation Principle in Control of Induction Motors*. Boston, MA: Kluwer, 1994.

[5] B. K. Bose, *Power Electronics and AC Drives*. Englewood Cliffs, NJ: Prentice-Hall, 1986.

[6] S. K. Sul and M. H. Park, "A novel technique for optimal efficiency control of a current-source inverter-fed induction motor," *IEEE Trans. Power Electron.*, vol. 3, no. 2, pp. 192–199, Apr. 1988.

[7] R. Marino, S. Peresada, and P. Tomei, "Adaptive output feedback control of current-fed induction motor," in *Proc. 12th IFAC World Congr.*, vol. 2, Sydney, NSW, Australia, Jul. 1993, pp. 451–454.

[8] ——, "Output feedback control of current-fed induction motor with unknown rotor resistance," *IEEE Trans. Contr. Syst. Technol.*, vol. 4, no. 4, pp. 336–347, Jul. 1996.

[9] K. Y. Lian and H. J. Tsai, "Adaptive control of current-fed induction motors with unknown rotor resistance," *J. Control Syst. Technol.*, vol. 4, pp. 245–255, 1996.

[10] R. Marino, S. Peesada, and P. Tomei, "Global adaptive output feedback control of induction motors with uncertain rotor resistance," *IEEE Trans. Automat. Contr.*, vol. 44, no. 5, pp. 967–983, May 1999.

[11] D. Kim, I. Ha, and M. Ko, "Control of induction motor via feedback linearization with input-output decoupling," *Int. J. Contr.*, vol. 51, pp. 863–883, 1990.

[12] J. Hu, D. M. Dawson, and Y. Qian, "Position tracking control of an induction motor via partial state feedback," *Automatica*, vol. 31, pp. 989–1000, 1995.

[13] D. Atkinson, P. Acarnly, and J. Finch, "Observers for induction motor state and parameter estimation," *IEEE Trans. Ind. Applicat.*, vol. 27, no. 6, pp. 1119–1127, Nov./Dec. 1991.

[14] S. Wade, M. W. Dunnigan, and B. W. Williams, "Modeling and simulation of induction machine vector control with rotor resistance identification," *IEEE Trans. Power Electron.*, vol. 12, no. 3, pp. 495–506, May 1997.

[15] X. Yu, M. W. Dunnigan, and B. W. Williams, "A novel rotor resistance identification method for an indirect rotor flux-orientated controlled induction machine system," *IEEE Trans. Power Electron.*, vol. 17, no. 3, pp. 353–364, May 2002.

[16] C. C. de Wit, H. Olsson, K. J. Åström, and P. Lischinsky, "A new model for control of systems with friction," *IEEE Trans. Automat. Contr.*, vol. 40, no. 3, pp. 419–425, Mar. 1995.

[17] Y. Tan and I. Kanellakopoulos, "Adaptive nonlinear friction compensation with parametric uncertainties," in *Proc. American Control Conf.*, San Diego, CA, Jun. 1999, pp. 2511–2515.

[18] C. C. de Wit and S. S. Ge, "Adaptive friction compensation for systems with generalized velocity/position friction dependency," in *Proc. 36th Conf. Decision Control*, San Diego, CA, Dec. 1997, pp. 2465–2470.

[19] C. C. de Wit and P. Lischinsky, "Adaptive friction compensation with partially known dynamic friction model," *Int. J. Adaptive Contr. Signal Process.*, vol. 11, pp. 65–85, 1997.

[20] K. M. Misovec and A. M. Annaswamy, "Friction compensation using adaptive nonlinear control with persistent excitation," *Int. J. Contr.*, vol. 72, no. 5, pp. 457–479, 1999.

[21] Y. Tan, J. Chang, and H. Tan, "Adaptive friction compensation for induction motors with inertia and load uncertainties," in *Proc. American Control Conf.*, Chicago, IL, Jun. 2000, pp. 615–620.

[22] M. Krstic, I. Kanellakopoulos, and P. Kokotovic, *Nonlinear and Adaptive Control Design*. New York: Wiley, 1995.

[23] H. K. Khalil, *Nonlinear Systems*, 2nd ed. New York: Macmillan, 1996.

Kuang-Yow Lian (S'91–M'94) received the B.S. degree in engineering science from National Cheng-Kung University, Tainan, Taiwan, R.O.C., in 1984 and the Ph.D. degree in electrical engineering from National Taiwan University, Taipei, in 1993.

From 1986 to 1988, he was a Control Engineer at ITRI. He joined Chung-Yuan Christian University, Chung-Li, Taiwan, in 1994, where he is currently a Professor and Chair for the Department of Electrical Engineering. His research interests include nonlinear control systems, fuzzy control, robotics, chaotic systems, and control system application.

Dr. Lian received the Outstanding Research Award from Chung-Yuan Christian University.

Cheng-Yao Hung was born in Taipei, Taiwan, R.O.C., in 1978. He received the B.S. degree from National Huwei Institute of Technology, Huwei, Taiwan, in 2000 and the M.S. degree from Chung-Yuan Christian University, Chung-Li, Taiwan, in 2002, where he is currently pursuing the Ph.D. degree, all in electrical engineering.

His current research interests include induction motor, linear induction motor, and nonlinear control theory.

Chian-Song Chiu (M'04) received the B.S. degree in electrical engineering and the Ph.D. degree in electronic engineering from the Chung-Yuan Christian University, Chung-Li, Taiwan, R.O.C., in 1997 and 2001, respectively.

He has been an Assistant Professor at Chien-Kuo Technology University, Changhua, Taiwan, since 2003. His current research interests are in robotics, fuzzy systems, and nonlinear control.

Peter Liu received the B.S. and Ph.D. degrees in electrical engineering from Chung-Yuan Christian University, Chung-Li, Taiwan, R.O.C., in 1998 and 2002, respectively.

He is currently an Embedded System Designer with applications in wireless communications with BenQ Corporation, Taipei, Taiwan. His research interests include chaotic systems, nonlinear control, and fuzzy systems.